Point defects in hexagonal boron nitride. II. Theoretical studies

A. Zunger
Department of Theoretical Physics, Soreq Nuclear Research Center, Yavne, Israel and Department of Chemistry, Tel-Aviv University, Ramat Aviv, Israel

A. Katzir
Department of Solid State Physics, Soreq Nuclear Research Center, Yavne, Israel
(Received 4 April 1974)

Substitutional and displaced carbon impurities and an isolated nitrogen vacancy in hexagonal boron nitride are theoretically investigated by the "small periodic cluster" approach. The perfect-solid band structure is calculated from the solution of the eigenvalues of a finite and periodic cluster of atoms arranged according to the known crystal structure. The linear combination of atomic orbitals representation of the crystal orbitals is adopted and semiempirical MO (molecular orbital) methods (extended Huckel, iterative extended Huckel) are used for the solution of the electronic eigenvalue problem. Point-defect problems are then treated by introducing the impurity atom or the vacant site into the otherwise perfect periodic cluster, and repeating the solution. Lattice relaxations are introduced around the defect site and charge redistribution among the cluster atoms is allowed for via self-consistent MO treatment. For a substitutional carbon impurity defect, it is observed that two deep defect levels, mainly localized on the carbon atom, appear (3.2–4.9 eV below the conduction band). Another level splits from the conduction band as the carbon atom is raised from the layer plane in a perpendicular direction. This level, 1.0–1.3 eV below the conduction band, has a symmetrical charge distribution on the three boron atoms surrounding the impurity site. As the distance of the carbon atom from the layer plane is increased to infinity, a nitrogen vacancy is formed. It is characterized by a defect level 1.1–1.4 eV apart from the conduction-band edge which also possesses a three-boron character. Lattice relaxations were shown to stabilize these defects. The findings agree semiquantitatively with the experimental results on these defects.

I. INTRODUCTION

In view of the accumulating experimental evidence indicating the participation of nitrogen vacancies and carbon impurities in determining optical, electron-paramagnetic-resonance (EPR), thermoluminescence, and photoluminescence properties of boron nitride (Paper I of this set), a theoretical calculation of these defects was undertaken. Based on known experimental data and previous theoretical studies of deep defects in covalent solids, the main requirements for such a theoretical defect model are the following: (i) It should locate the position of the defect levels with respect to the band edges. The energy separation between the defect level and the band edges should then be compared with EPR and thermoluminescence activation energies and with the temperature dependence of photoluminescence. (ii) It should provide the electronic wave function of the defect level, and thus the charge distribution around the defect site, to be compared with both the EPR assignment and the hyperfine splitting. (iii) Due to both the presence of ionic-covalent bonding in the perfect crystal and to charge redistribution induced by the vacancy or the impurity in the defect structure, the model should provide a self-consistent picture of the electron distribution relative to the separated atoms and unperturbed lattice. (iv) Since σ-π coupling effects were shown to modify the bandwidth[1–4] and the self-consistent atomic charges[2,3] significantly, the model should incorporate all the valence electrons on the same level of approximation. The σ electrons do not behave as an unpolarized core and thus the treatment of π electrons alone can lead to erroneous results.[5] (v) Since lattice distortions in covalent solids around the defect site were shown to modify the deep defect levels[6,7] significantly, the model must provide a way of introducing lattice relaxations. (vi) In view of the relative paucity of experimental data on the perfect boron-nitride crystal, a reliable model based on parametrizing the theoretical variables in accord with experimental band structure[8,9] cannot be employed. (vii) Due to significant charge delocalization in planar π-electron systems, the model should account for the coupling of the defect electrons with a relatively large portion of the bulk of the crystal.[10]

Theories that start from the periodic Bloch states of the perfect crystal and introduce the defect perturbationally[11–13] satisfy conditions (i), (iv), and (vii) but supply little information on requirements (ii) and (v). On the other hand, theories that construct the defect levels from the orbitals of the local environment (usually nearest neighbors only) of the defect [10,14,15] meet conditions (ii)–(v) but are deficient in satisfying conditions (i), (vi), and (vii). Effective-mass theories [16,17], that have been shown to be useful in describing shallow traps, fail to ac-

count for deep levels in semiconductors mainly due to the neglect of lattice relaxations. Simple Huckel-type π-electron calculations[5,18,19] satisfy conditions (ii), (v), and (vii), but grossly neglect conditions (i), (iii), (iv) and (vi). Point defects in hexagonal BN have been treated so far only by this method.[5,19]

Truncated crystal models[2,20-25] which use either semiempirical linear-combination-of-atomic-orbitals (LCAO) methods[26-28] or the $X\alpha$ scattered-wave technique,[29] automatically satisfy conditions (iv) and (vi), and the practical possibility of incorporating a relatively large number of atoms in the model with moderate computer time, satisfies condition (vii). Its major disadvantage lies in the fact that the energy bands are not well defined[22,24] and that due to the presence of many "dangling" bonds on the cluster's surface significant charge inhomogeneity is present over each sublattice.[24,30]

In recent works of Watkins and Messmer[31,32] on diamond and Zunger[3,33] on graphite and boron nitride, different approaches were suggested to avoid the problems of charge inhomogeneity and lack of straightforward correlation between the perfect crystal and defect energy levels. These methods use a superlattice representation to the defect structure by either using a reciprocal-space tight-binding approach with the defect placed at the center of a large unit cell,[31,32] or by considering a finite periodic cluster of atoms with a defect placed in its center, in a real-direct-space approach.[3,33] These methods could be implemented in practice with the aid of large computers and satisfy the requirements previously stated.

In this paper we treat the problems of substitutional carbon impurity, displaced carbon impurity, and nitrogen vacancy in hexagonal boron nitride, using both the truncated-crystal and the "small-periodic-cluster" methods. The essential features of both methods are discussed in Sec. II. A critical examination of them is provided in Sec. III, where comparison with experimental data is made.

Due to the complexity involved with *ab initio* calculations of such models, semiempirical all-valence-electron methods are usually employed. In view of the experience gained with these methods in molecular calculations, it seems dangerous to adopt exclusively only one of these approximations in calculating solid-state properties. Consequently we examine some of the common semiempirical methods for both the perfect crystal and the defect structures. Problems regarding the convergence of the obtained electronic structure are also discussed.

II. METHODS OF CALCULATION

A. Truncated-crystal method

In the truncated-crystal approach, a cluster of N atoms arranged spatially according to the crystal geometry is considered. A crystal orbital ϕ_i is represented in the LCAO approach as a linear combination of η atomic orbitals (usually valence orbitals are used) centered on the N atoms of the cluster:

$$\phi_i = \sum_{\nu=1}^{\eta}\sum_{n=1}^{N} C_{\nu n i}\,\chi_\nu(\vec{r}-\vec{R}_n), \tag{1}$$

where $\chi_\nu(\vec{r}-\vec{R}_n)$ represents an atomic orbital ν centered on site n. The coefficients $C_{\nu n i}$ are the solutions of the one-electron Hartree-Fock equations, given by

$$\sum_{m}^{N}\sum_{\nu}^{\eta}(F_{\mu n,\nu m}-S_{\mu n,\nu m}\epsilon_i)\,C_{\nu m i}=0, \tag{2}$$

where the matrix elements in the atomic orbital basis are given by

$$F_{\mu n,\nu m}=\langle\chi_\mu(\vec{r}-\vec{R}_n)|\hat{F}|\chi_\nu(\vec{r}-\vec{R}_m)\rangle,$$
$$S_{\mu n,\nu m}=\langle\chi_\mu(\vec{r}-\vec{R}_n|\chi_\nu(\vec{r}-\vec{R}_m)\rangle, \tag{3}$$

and $\hat{F}$ is the Hartree-Fock one-electron operator. The perfect-cluster eigenvalues are calculated by solving Eq. (2) with an atomic valence basis set ($|\nu\rangle = 2s,\ 2p_x,\ 2p_y,\ 2p_z$) for several values of N, in order to obtain the convergence limit of the one-electron eigenvalues. The resultant eigenvalues for a small cluster generally do not correspond to energy levels in the Brillouin zone(BZ) of the infinite periodic crystal. It was previously shown however,[2,3] that for layered hexagonal lattices of D_{6h} or D_{3h} point symmetry, such as in two-dimensional graphite and boron nitride, respectively, it is possible to select planar geometries in such a way that each eigenvalue of its electronic secular determinant corresponds to an energy level in the BZ of the infinite lattice. This is true provided the matrix elements of Eq. (3) have already assumed their bulk value due to introduction of sufficient nearest-neighbor interactions, and that surface effects can be neglected. Thus one is able to calculate approximately the band edges and band width of the ideal infinite crystal as well as other high-symmetry $\vec{K}$-points, by considering finite clusters. Point-defect levels are then calculated by substituting a guest atom for a particular cluster atom (substitutional impurity) or rejecting one atom from the cluster (point vacancy) and repeating the eigenvalue calculation. The new eigenvalue spectrum is analyzed and the defect levels appearing in the forbidden gap (which have no counterpart in the ideal-cluster spectrum) are investigated as a function of lattice distortions around the defect site. The charge associated with such a level is calculated from the coefficients $\{C_{\nu n j}\}$ of the correspond-

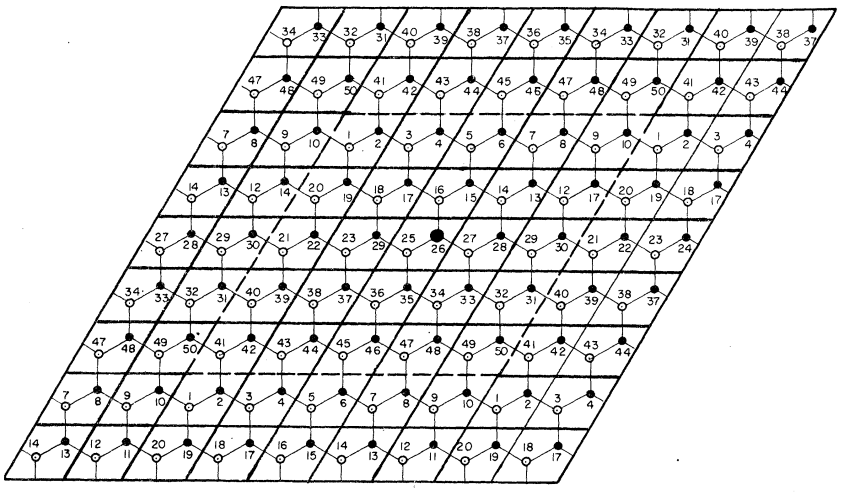

FIG. 1. Fifty-atom molecular cluster (surrounded by dashed lines) and the extracluster atoms (atoms between dashed and heavy lines) used to establish a periodic interaction geometry. The central atom (atom 26, marked by heavy circle) has no interaction with an identical atom in the extracluster region.

ing level ϕ_j through standard[34] or modified[35] population analysis. The dangling bonds that appear on the surface of the cluster, are either saturated by attaching hydrogen atoms[2,24] or treated as free bonds.[21-23,36]

B. Small-periodic-cluster method

In the small-periodic-cluster (SPC) method, one constructs a *periodic* cluster of N atoms (refered here as the molecular cluster) that is arranged spatially according to the lattice symmetry of the chosen structure. Since the matrix elements of Eq. (3) appearing in the Hartree-Fock equations [Eq. (2)] depend only on the *relative* orientations of pairs of atoms, it is sufficient to specify an interatom-distance matrix $D^{(N)}_{m,n}$ for the N-atom cluster and three interatom direction-cosine matrices $E^{(N)}_{m,n}(x)$, $E^{(N)}_{m,n}(y)$, and $E^{(N)}_{m,n}(z)$ relative to arbitrary x, y, and z directions. The absolute atomic coordinates, with reference to a fixed origin, need not be specified in order to obtain the solution to the eigenvalue problem of an isolated molecular system. This freedom in describing the crystal structure can be used to construct these matrices as cyclic matrices appropriate for a "pseudomolecule" that is *periodic* in space, and keeps the correct geometry of a given lattice. The range of interaction $\lambda(N)$ in such an N-atom periodic cluster is determined solely by the symmetry of the lattice and by N, e.g., a cluster made up of $N = 2\lambda + 1$ atoms can be used to represent a periodic one-dimensional lattice with interaction range $\lambda(N)$, and clusters of D_{3h} or D_{6h} symmetry with 8, 18, 32, 50 etc. atoms for example, could be used to present a periodic hexagonal structure with 1, 2, 3, and 4 orders of interactions, respectively. Figure 1 shows a 50-atom hexagonal molecular cluster (surrounded by the dashed parallelepiped) that is made of 5×5 hexagonal unit cells with 2 atoms per cell. Extension of this cluster by two rows of hexagonal cells in the two planar directions (the cells between the dashed and heavy outer lines) is denoted as the extracluster region. Truncation of the interaction between each two atoms, either inside the central cluster or between an atom in the cluster and an atom in the extra-cluster region, to a range of $\lambda(50)\leq 4$, defines a *periodic* hexagonal "interaction geometry." The distance matrix $D^{(N)}$ is constructed to define this interaction geometry in terms of the nearest-neighbor distance R_{BN} while the direction-cosine matrices define the hexagonal point symmetry in terms of the hexagonal angle. These matrices are used to construct the Hartree-Fock matrix elements $F_{\mu n,\nu m}$ and $S_{\mu n,\nu m}$ for a minimal basis set of atomic orbitals, generating thereby a Hermitian eigenvalue problem. The crystal orbitals of such periodic clusters are thus constructed as in Eq. (1), but the lattice vectors $\vec{R}_n$ are now restricted to represent the periodic finite structure of interaction range $\lambda(N)$.

The eigenvalues of Eq. (2) are first solved for a regular perfect lattice. At this limit, the eigenvalues are simply analyzed according to the wave vector $\vec{K}_p$ in the BZ by recognizing that the solutions could be usually represented (by decomposing the crystal orbital index i to its components $i \equiv \alpha p$, where $\alpha = 1 \cdots \eta$; $p = 0 \cdots N-1$) as:

$$C_{\nu ni} \equiv C_{\nu n\alpha p} = C_{\nu n\alpha p} e^{i\vec{K}_p \cdot \vec{R}_n},$$
$$\epsilon_i \equiv \epsilon_{\alpha p} = \epsilon_\alpha(\vec{K}_p), \tag{4}$$

where $\vec{K}_p = (2\pi/N\vec{b})p$ and $\vec{b}$ is a primitive lattice vector. The band structure $\epsilon_\alpha(\vec{K}_p)$ is obtained as a discrete subset of the infinite crystal spectrum at N/h $\vec{K}$-values, evenly spread in the BZ, where h is the number of atoms in the basic unit cell ($h = 2$ for graphite and boron nitride).

The total ground-state energy is obtained in the

simple one-electron picture as

$$E_{\text{tot}} = 2 \sum_{\alpha}^{\sigma_{\text{oc}}} \sum_{\vec{K}_p}^{N} \epsilon_\alpha(\vec{K}_p) \tag{5}$$

where σ_{oc} denotes the highest occupancy. The stable crystal conformation under static equilibrium is then obtained by minimizing E_{tot} with respect to the nearest-neighbor distance R_{BN} and by examining the stability of the total energy against displacement of a specific atom.

The resulting equilibrium value of R_{BN} is compared with crystallographic data while the cohesive energy at equlibrium is compared with the experimental thermochemical determination. The stretching force constant is obtained by performing numerical derivatives of the total energy at the static equilibrium conformation with respect to symmetry-stretching coordinates and comparing with the experimental data from band spectra. The resulting wave functions are subjected to a population analysis to determine orbital and net atomic charges to be compared with nuclear quadrupole resonance (NQR) data.

The convergence problems encountered in the model are (a) convergence of the matrix elements in Eq. (3) as a function of the interaction order $\lambda(N)$ employed [Eq. (5)], (b) convergence of the total energy as a function of the $\vec{K}$ grid used for each cluster size, (c) convergence of the self-consistent-field (SCF) iteration cycle when the energies are computed with a self-consistent LCAO method.

Due to numerical difficulties the convergence of the band structure as a function of the size η of the atomic set employed will not be examined, and a valence basis set will be used throughout.

The fact that the 3*s* orbital energies of free boron and nitrogen atoms are well separated from the valence orbital energies suggests that no substantial mixing should occur in the valence bands while the conducting states could be affected by introducing virtual orbitals.

The convergence problems (a) and (b) could be reduced to one, if we use the maximum interaction range allowed for a cluster of a given size N. In this case both $\lambda_{\text{max}}(N)$ and the size of the $\vec{K}$ grid are uniquely determined by N. The size of the cluster is chosen so that one will satisfy the convergence problems (a) and (b) within a prescribed tolerance and that the $\vec{K}_p$ subset will contain high-symmetry points that are of interest in analyzing optical and energy-loss data concerning band-to-band transitions. It was previously shown[2] that a 18-atom periodic cluster arranged in D_{3h} or D_{6h} geometry contains in its eigenvalue spectrum the Γ and P points (notation of Bassani and Parravicini[9]) while a 32-atom periodic cluster also contains the Q saddle point. Optically allowed transitions in both graphite and boron nitride are related to these high-symmetry points.[9]

Employing a self-consistent solution to the N-atom periodic cluster is equivalent to sampling a maximum of N/h $\vec{K}$ points in computing the crystal potential in a self-consistent approach for infinite crystals.[37,38] It has been previously shown[39–41] that constructing the crystal potential as a superposition of free-atom potentials without recompiling it on the basis of the calculated band structure at several selected $\vec{K}$ points, result in a poor approximation to the self-consistent results in systems exhibiting some polarity (deviations of 1–5 eV in the band energies of binary II-VI crystals).

In self-consistent orthogonalized-plane-wave (OPW) calculations, the contribution of only 2–4 states of the entire BZ to the charge density were shown to be sufficient to correct in some cases the non-self-consistent potential. In the small-periodic-cluster (SPC) approach a larger number of states (in the nondegenerate case, N/h different states) are incorporated automatically in the evaluation of the potential at each iteration. Moreover, these states are evenly spread in the BZ and are not subjected to somewhat arbitrary choice of the $\vec{K}$ grid, as in methods that factorize the secular equations utilizing explicitly the lattice translational symmetry in constructing the crystal functions.

Since in the formulation of the eigenvalue problem of the central molecular cluster we do not impose explicit translational symmetry on the eigenfunctions inside the large Born–von Karman cell, the SPC method could be easily extended to treat point-defect structures in the representation of a rather dilute defect superlattice. This is done by removing the *central* cluster atom (e.g., atom 26 in Fig. 1) to infinity, creating thereby a point vacancy, or by changing its chemical identity and generating a point impurity. It should be noted that when the molecular cluster is composed of an odd number of hexagonal unit cells (e.g., 18-atom cluster with 3×3 or 50-atom cluster with 5×5 unit cells), the central atom in this cluster has no direct interaction with an equivalent atom in the extra cluster region since the periodicity of the structure is already satisfied by applying only intracluster interactions for this atom. This suggests that the superlattice representation of the defect problem in this model should not place a too severe restriction when comparison is made with experimental data concerning dilute defects, since the dispersion of the defect band is induced only by the relatively small polarization effects of the guest atoms on the charge density of the host atom. These polarization effects, being generally of short range, could then be easily suppressed by increasing the cluster size, thus reducing the interaction range.

The defect levels, the charge distribution on them, and their location relative to the band edges are thus calculated on the same level of approximation as the perfect crystal bands and charges, enabling thereby a straightforward comparison between them.

The main advantages of the small-periodic-cluster approach over the truncated-crystal method are (a) The one-electron levels of the perfect periodic cluster are related in a simple way to well defined points in the band structure of the infinite solid; (b) Charge homogeneity over each sublattice in the perfect periodic lattice is guaranteed by the fact that each atom in the cluster experiences the same crystalline environment as the others, and no dangling bonds appear. *Ad hoc* treatment of the surface is not needed; (c) A self-consistent evaluation of the crystal potential, involving a relatively large number of crystal states, is feasible.

The model is preferable to the "defect-molecule" approach[10,15] since it allows coupling of the defect with a relatively large portion of the bulk solid, thereby allowing for a larger delocalization space for the defect electrons, and it relates the defect energy levels to the band levels. The advantages over the methods that start from perfect periodic lattice states[11–13] lie in the fact that lattice relaxations can easily be introduced here, while in the previous methods these will cause a significant increase in the perturbative effect induced by the defect on the periodic states. Also the charge distribution in the defect level is simple to calculate by this method using straightforward population analysis on the resulting wave functions.

The main disadvantages of the small periodic cluster approach are the following:

(i) It involves solutions of large electronic secular determinants (for a 32-atom cluster with four atomic valence orbitals on each atom, 128×128 matrices are treated) since translational symmetry is not explicitly utilized, but in turn, a more realistic description of deviation from periodicity is possible.

(ii) It does not yield results that are continuous in the wave vector $\vec{K}$, but rather a discrete subset is obtained. Thus, the density of states cannot be reliably calculated.

(iii) The defects electronic properties are described in a superlattice representation with a cluster-size dependence of the indirect defect-defect interactions.

Since the SPC method is more useful than the truncated-crystal method, the latter will be used only to a limited extent.

C. Semiempirical LCAO computation schemes

Due to the complexity of *ab initio* calculations of all the $F_{\mu n,\nu m}$ elements, some semiempirical methods are used to calculate these elements approximately. In the extended Huckel (EXH) approximation[26] the matrix elements are given by

$$F_{\mu n,\nu m}=0.5G(F_{\mu 0,\mu 0}+F_{\nu 0,\nu 0})S_{\mu n,\nu m}\ ,$$

where $S_{\mu n,\nu m}$ are the atomic overlap intergrals calculated from Slater atomic orbitals, $F_{\mu 0,\mu 0}$ and $F_{\nu 0,\nu 0}$ are atomic orbital energies of orbitals μ and ν, respectively, taken from Hartree-Fock calculations on free atoms or alternatively from atomic spectra. G is a semiempirical constant chosen to fit some electronic properties of medium to large molecules, and usually taken to be 1.75.[26]

The derivation of the EXH approximation from the Hartree-Fock equations was given by Blyholder and Coulson[42] and by Gilbert.[43] For systems with moderately uniform charge distribution (a difference of less than 1.3 in the electronegativities of the atoms in Pauling's scale, compared with a difference of 1.0 between N and B), this was shown to be a reasonable approximation to the rigorous Hartree-Fock scheme.

Since in general the Hartree-Fock operator $\hat{F}$ couples electronic contributions to the potential from *all* atoms and orbitals in the cluster (and not only from a particular $\mu n,\nu m$ pair), it depends on the charge distribution of all electrons and nuclei. A semiempirical self-consistent approach to Eqs. (2) and (3) [iterative extended Huckel (IEXH)[27,35]], which is a refinement over the non-self-consistent EXH approach and does not contain a free parameter is characterized by an iterative solution, in which the diagonal $F_{\nu n,\nu n}$ elements are taken to be explicitly charge dependent:

$$\begin{aligned} F_{\nu n,\nu n}&=F^{o}_{\nu n,\nu n}+Q_n\Delta F_\nu\ ,\\ F_{\mu n,\nu m}&=S_{\mu n,\nu m}(F_{\mu n,\mu n}+F_{\nu m,\nu m})(1-0.5|S_{\mu n,\nu m}|)\ . \end{aligned} \tag{6}$$

$F^{o}_{\nu n,\nu n}$ is the atomic orbital energy of the free atom, Q_n is the net atomic charge on the atom n, calculated from the solutions $\{C_{\mu ni}\}$ of Eqs. (1) and (2) for all occupied states. ΔF_ν is the change in the ν-orbital potential due to deviation from charge neutrality (ionicity), as calculated from the Hartree-Fock orbital energies of free ions of different ionization states or taken from atomic spectra. According to this procedure one guesses Q_n values for all the atoms (usually the initial guess for systems that are only partially ionic is the free atom value $Q_n=0$). Then the matrix elements of Eq. (3) are constructed and solved for the coefficients $\{C_{\nu ni}\}$ of Eq. (2), and the atomic charges are calculated from the wave functions. A damping procedure is used to faciliate the convergence of the iteration cycle.[35]

The atomic orbital energies were taken from the original work of Hoffman[44] and the ΔF_ν values were taken from the interpolation scheme of Cusachs and

Reynolds.[45] The atomic orbitals were taken as Slater orbitals with the usual Slater exponents. Interaction and overlap matrix elements between the N atoms are evaluated up to three to four orders of neighbors in the SPC method and between all atoms in the cluster in the truncated-crystal approach. No adjustment of the semiempirical constants to obtain better agreement with experiment[31] is performed. The iteration cycle in IEXH calculation are terminated when the difference between atomic charges on successive iterations does not exceed $10^{-2}e$. Under these conditions, the band structure and total energy per BN pair satisfy the first three convergence requirements previously mentioned to within less than 0.1 eV.

D. Electronic properties of the perfect crystal

The calculated band structure of the perfect hexagonal lattice of boron nitride using IEXH method and an 18-atom cluster ($\lambda = 2$; P, and Γ points included) was previously[3] compared with both experimental data and with other non-self-consistent tight-binding calculations.[1,8,46] To examine the convergence properties of the results, we have performed these calculations on an eight-atom cluster ($\lambda = 1$; Q, and Γ points included) and on a 32-atom cluster ($\lambda = 3$; Q, and Γ points included). Relatively small differences occur upon increasing the interaction range: the $\pi \rightarrow \pi^*$ band-to-band transition at the Q_2^- points in the BZ is shifted from 5.8 eV at $\lambda = 1$ to 6.0 eV at $\lambda = 3$ [experimental electron energy-loss data indicate $\simeq 6.2$ eV (Ref. 47)], the bottom of the lowest valence band occurring at the Γ_1^+ point is 18.46 eV away from the center of the band gap for the $\lambda = 1$ calculation, 18.81 eV for the $\lambda = 2$ calculation, and 18.86 eV for the $\lambda = 3$ calculation [electron-scattering data give 19.4 eV (Ref. 48]. The lowest $\sigma \rightarrow \sigma^*$ transition ($Q_2^+ \rightarrow Q_1^+$) occurs at 13.9 eV in the $\lambda = 1$ calculation and at 14.1 eV in the $\lambda = 3$ calculation [energy-loss data indicate 14.1 eV (Ref. 47) to 10.1 eV (Ref. 49)] while the lowest mixed $\sigma \rightarrow \pi^*$ transition ($Q_2^+ \rightarrow Q_2^-$) occurs at 8.8 eV in the $\lambda = 1$ and 8.9 eV in the $\lambda = 3$ calculation [energy-loss data give ~ 9.4 eV (Ref. 47)]. The band gap is obtained only in the 18-atom cluster calculation as 3.7 eV [experimental optical and photoelectron data are scattered between 5.4 to 3.6 eV (Refs. 50–52)]. The binding energy changes from 6.6 eV in the $\lambda = 1$ case through 7.2 eV in the $\lambda = 2$ calculation to 6.7 eV in the $\lambda = 3$ calculation (compared with 6.6 eV obtained in thermochemical determination[53]). This nonmonotonic behavior results from the fact that the 8- and 32-atom clusters include the Q saddle point that contributes a large part of the cohesive energy due to its high degeneracy, while the 18-atom cluster includes band-edge points with low degeneracy. Optimization of the total energy with respect to the nearest-neighbor BN distance yields equilibrium values of 1.441 Å in the $\lambda = 2$ case and 1.449 Å in the $\lambda = 3$ case [compared with the crystallographic determination of 1.446 Å (Ref. 54)]. The stretching-force constant is calculated to be 10.1×10^5 dyn/cm and 10.8×10^5 dyn/cm for the $\lambda = 2$ and $\lambda = 3$ calculations, respectively (compared to $\sim 8.3 \times 10^5$ dyn/cm obtained from band spectra[55]). The boron π charge is calculated to be $0.52e$ and $0.50e$ in the $\lambda = 2$ and $\lambda = 3$ calculations, respectively [NQR results yield $0.45e$ (Ref. 56)]. The convergence of these electronic and structural features seems thus to be obtained at about $\lambda = 2$–3.

Repeating these calculations with the EXH scheme, a similar convergence rate is obtained. The results exhibit however some pronounced differences relative to the IEXH results. The results obtained with the largest clusters are: a $\pi \rightarrow \pi^*$ transition at 6.29 eV, the Γ_1^+ point at 19.0 eV, a $Q_2^+ \rightarrow Q_1^+$ transition at 15.0 eV, a $Q_2^+ \rightarrow Q_2^-$ transition at 9.4 eV, a gap of 5.49 eV, binding energy of 6.04 eV, equilibrium B–N bond length of 1.443 Å, boron π charge of $0.31e$ and a stretching-force constant of 13.1×10^5 dyn/cm. Truncated-crystal results for boron nitride have been previously published[2] and seem to be in poorer agreement with experiment for reasons discussed above.

It is quite unfortunate that in view of the large uncertainties in optical and energy-loss data for boron nitride and the paucity of experimental data on transitions at higher energy and on effective charges, it is difficult to decide at this stage which LCAO scheme should be preferred. It seems however that the extended-Huckel method is better for describing energies while the iterative-extended-Huckel method is better for determining charges and atomic orbital coefficients. Similar conclusions were previously suggested from extensive comparison of these methods in predicting various properties of molecules.[57] The IEXH is more difficult to implement in practice due to higher computer time requirements. Consequently, in the following work we use EXH and IEXH methods for 18- and 32-atom clusters while a limited number of calculations on the 50-atom cluster will be performed only with the EXH method.

III. RESULTS

A. Substitutional carbon impurity in hexagonal boron nitride

Table I summarizes the calculated results for a substitutional carbon impurity in two-dimensional hexagonal boron nitride as computed by the truncated-crystal and small-periodic-cluster methods with the EXH approximation. The results for an ideal cluster without a defect and for the cluster with the defect are compared. The truncated clusters used for the calculation were $B_{10}N_{12}H_{12}$,

TABLE I. Calculated results for a substitutional C impurity in hexagonal boron nitride, obtained using the EXH method. E_C^σ, E_C^π, and E_C^{2s} represent energy levels appearing due to the carbon impurity. ΔE_{v-d} represents the energy difference between the edge of the conduction band and the highest defect level. Q_C^π denotes the carbon π charge. Cluster I: $B_{10}N_{12}H_{12}$, cluster II: $B_{12}N_{12}H_{12}$, cluster III: $B_{14}N_{14}H_{14}$ (see Fig. 2).

	Truncated crystal						Small-period clusters			
	Cluster I		Cluster II		Cluster III		18 atoms		32 atoms	
Property	No. defect	Carbon impurity	No. defect	Carbon impurity	No. defect	Carbon impurity	No. defect	Carbon impurity	No. defect	Carbon impurity
Valence edge (eV)	−12.675	−12.921	−12.762	−12.983	−12.598	−12.832	−11.960	−12.731	−11.962	−12.735
Conduction edge (eV)	−7.210	−7.210	−7.269	−7.269	−7.155	−7.155	−6.470	−6.470	−6.471	−6.471
Band gap (eV)	5.465		5.493		5.443		5.490		5.491	
E_C^σ (eV)		−12.042		−11.931		−11.913		−11.340		−11.345
E_C^π (eV)		−12.140		−12.140		−12.135		−12.129		−12.127
E_C^{2s} (eV)		−23.340		−23.285		−23.199		−23.150		−23.150
ΔE_{v-d} (eV)		4.832		4.871		4.758		4.879		4.874
Q_C^π (e)		−1.468		−1.467		−1.467		−1.467		−1.467
% C character										
in E_C^σ		40.09		40.10		40.12		40.12		40.15
in E_C^π		66.12		65.31		64.45		65.21		64.92
in E_C^{2s}		98.39		86.65		96.35		97.10		97.12

$B_{12}N_{12}H_{12}$, and $B_{14}N_{14}H_{14}$ (Fig. 2).

It is seen that upon substitutionally introducing a carbon atom instead of a nitrogen atom in the hexagonal network, three new one-electron levels appear. The lowest of them (E_C^{2s}) is a level mainly composed of the 2s atomic orbitals of the carbon atom and highly localized (more than 96% carbon character, Table I) at the carbon site. This level is slightly stabilized when compared with the free carbon 2s state, and behaves actually as a core state. The three degenerate 2p orbitals of the free carbon atom are split in the crystal (which has a D_{3h} point symmetry) into two crystal-field components: a doubly degenerate σ level (E_C^σ) spread in the layer plane, and a π level (E_C^π) perpendicular to the layer plane. The E_C^σ state contains 40% of carbon $2p_x$ and $2p_y$ character, and due to mixing with the corresponding σ orbitals of the boron and nitrogen atoms, its energy is stabilized by more than 0.5 eV compared with the corresponding level in the free atom. The E_C^π level is slightly more stabilized than the E_C^σ level, due to a relatively higher delocalization of π electrons in the crystal plane. In the perfect lattice the larger delocalization of the π electrons results in higher electrical conductivity in this direction.

The edge of the conduction band remains unchanged upon introducing the impurity, while the edge of the valence band, corresponding to the work function of the solid, decreases slightly. The difference ΔE_{v-d} between the highest impurity level E_C^σ (which is only singly occupied in the neutral state) and the edge of the conduction band is only slightly affected by increasing the cluster size and assumes a value of about 4.8 eV, as can be seen from Table I.

The carbon impurity level E_C^σ acts therefore as a deep acceptor level that can capture free carriers, thereby decreasing their degree of delocalization. It also decreases the optical gap, shifting the wavelength of the absorbed light towards the visible (coloring effect). Such a trend was experimentally observed in carbon-doped boron nitride.[58] Analysis of the ideal crystal band structure[2,3] reveals that the edge of the conduction band (P_2^- point) is composed of boron π orbitals (99.43% boron π character in cluster III, and 100% boron π character in SPC representations). The optical transition from the carbon impurity level to the conduction band edge is therefore an internal charge-transfer transition similar to those encountered in molecular spectroscopy.[59] Such a transition carries the electron from a level localized to a large extent on the carbon atom, to a level spread over the boron sublattice. This should be contrasted with the lowest transition of the pure crystal which carries the system from a level delocalized on the nitrogen sub-

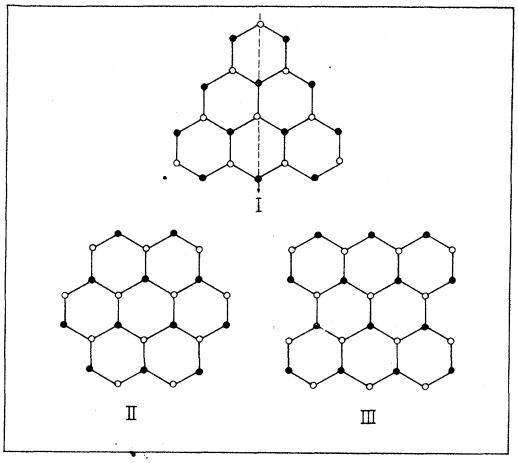

FIG. 2. BN clusters used in the truncated-crystal calculations. Each cluster is surrounded by H atoms to satisfy the free valence. $R_{BN}=1.446$ Å, $R_{BH}=1.2$ Å, and $R_{NH}=1.1$ Å. Cluster I: $B_{10}N_{12}H_{12}$ or $B_{12}N_{10}H_{12}$; Cluster II: $B_{12}N_{12}H_{12}$, Cluster III: $B_{14}N_{14}H_{14}$. ●: boron; ○: nitrogen.

lattice (the P_1^- edge of the valence band) to a level delocalized on the boron sublattice (the P_2^- state).

Comparison between the results obtained by the truncated-crystal and the small-periodic-cluster methods indicates that in the former method the edges of the valence and conduction bands are changed nonmonotonically with increasing cluster size, and these edges can thus be only approximately determined by this method. A similar behavior was observed by Larkins[24] and by Messmer and Watkins[22] in calculating the electronic eigenvalue spectrum of diamond and siliconlike atomic clusters, and by Zunger[2] in a truncated-crystal calculation for graphite. The calculation of atomic charges in the perfect periodic cluster reveals complete homogeneity of charges on each sublattice, while in the truncated-crystal model, strong perturbations in the charge are evident near the boundaries of the cluster.

In both truncated-crystal and SPC calculations, the carbon atom accumulates a large negative charge ($Q_C^{net} = 0.88e$) at the expense of the surrounding boron atoms, due to the greater electronegativity of carbon. This charge transfer is carried out in a substantial way through the π system, resulting in a carbon π charge of $1.467e$ (compared to $1.222e$ in a similar SPC EXH calculation on graphite). The extent of this effect is probably overestimated in a non-self-consistent treatment such as EXH, and a charge iterative calculation should be applied to achieve more accurate results. We recalculated the 18- and 32-atom periodic cluster problem now employing the self-consistent IEXH method. The highest carbon impurity level E_C^σ obtained when the carbon impurity calculation is performed is now 2.2 eV and 2.1 eV below the conduction edge for the 18- and 32-atom clusters, respectively. The carbon atom is shown to have a net atomic charge of $-0.28e$. The general features of the non-self-consistent treatment are preserved, but considerable quatitative differences occur due to the requirement of self-consistent charge redistribution. Similar differences between non-self-consistent and self-consistent band energies were calculated by Stukel *et al.*[41] on binary II-VI crystals, by the OPW method.

It should be noted that the level splitting and ordering obtained here for the C-impurity model indicate that such a system will exhibit dielectric losses, as argued by Sussman.[60]

We next allow for model lattice relaxations around the C impurity, using the self-consistent IEXH method. An inward relaxation of 18% of the bond length, along the bonding distance, of the three boron atoms surrounding the impurity, lowered the energy of the clusters to a minimum. The gap between the highest defect level and the conduction edge increases now to 3.2 eV. This large effect demonstrates the importance of such processes in deep defect levels in covalent and partly ionic crystals. Thd fact that the IEXH method, when applied to the 18- and 32-atom perfect BN clusters, reproduces the equilibrium interatom distance and stretching-force constant reasonably well, justifies its use in investigating model relaxations. The negative net atomic charge on the central carbon atom increases to $-0.35e$ upon relaxing the boron atoms, the carbon thus assumes a greater stabilizing electrostatic interaction with the boron atoms.

A similar relaxation calculation with EXH method reveals a change in E_{v-d} from 4.8 to 4.9 eV and a change in carbon net charge from $-0.88e$ to $0.90e$. When the carbon atom impurity lying in the lattice plane is moved from the proper D_{3h} site (occupied by a nitrogen atom in the ideal cluster), the twofold degeneracy of the E_C^σ level is lifted. The total lattice energy increases, however, relative to the D_{3h} impurity, and therefore no detailed mapping of the potential surface was made. The separation E_{v-d} of the defect level from the conduction band is affected only slightly by cluster size. A calculation of an unrelaxed 50-atom cluster with the EXH method yields $E_{v-d} = 4.882$ eV compared with the value $E_{v-d} = 4.879$ eV for the 18-atom cluster.

B. Displaced carbon impurity in hexagonal BN

We next investigated the nonsubstitutional carbon defects. These are characterized by a carbon atom replacing a nitrogen atom and located at distance R_C above the vacant site and perpendicular to the lattice plane ($R_C = 0$ is thus the planar impurity case). The calculations are performed on the 18-atom periodic cluster with the EXH approximation for the matrix elements. Figure 3 shows some of the relevant one-electron energy levels as a function of R_C.

The pronounced features are the following.

(a) A conduction-band level (denoted E_t) splits from the conduction band as the distance of the carbon atom from the vacant site increases. The charge carried by this level is mainly located symmetrically with respect to the carbon atom and its three equivalent nearest-neighbor boron atoms. The distance of this level from the conduction edge tends to level off for large R_C. For $R_C = 1.0$ Å it is at 1.30 eV from the conduction band. The contribution of the defect orbital to the charge on the three boron atoms surrounding the carbon impurity decreases with increasing R_C. For $R_C = 1.0$ Å this charge is $0.36e$.

(b) The crystal-field splitting between the E_C^σ and E_C^π levels decreases with increasing R_C. Both levels are destabilized as R_C increases, thus approaching their free atom degenerate state.

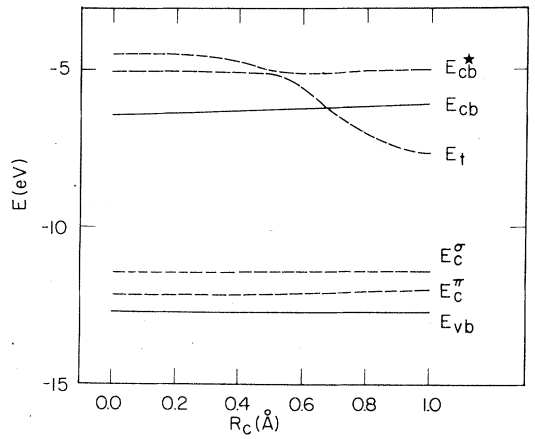

FIG. 3. Dependence of one-electron energies on the perpendicular distance R_C of the carbon impurity from the vacant nitrogen site. E_{cb} and E_{vb} denote conduction and valence band edges, respectively. (E_{cb}^{*} denotes a higher conduction state.) E_t denotes the trapping level and originating from the $\Gamma - Q$ line in the perfect solid, and E_C^{σ} and E_C^{π} denote the carbon impurity σ and π levels, respectively.

(c) The edges of the conduction band (E_{cb}) and valence band (E_{vb}) are slightly shifted as R_C increases.

Similar results are obtained with IEXH method, the defect level lying now at 1.0 eV and contribution a charge of 0.29e to the boron atoms for R_C = 1.0 Å.

In the neutral impurity state, the level E_C^{π} is doubly occupied, E_C^{σ} is singly occupied, and E_t is empty. This last level could act as an electron trap and would then exhibit a characteristic three boron EPR signal due to the even distribution of charges on the three boron atoms surrounding the vacant site. Its energy below the conduction band suggests that it should also give rise to thermoluminescence effects with an activation energy of $-E_t - E_{cb} \approx 1.0-1.3$ eV. This is consistent with the model proposed to explain the role of carbon impurities in BN (see Paper I).

When the distance R_C is further increased, the binding energy of the carbon atom to the hexagonal lattice (0.64 eV for $R_C = 0$) decreases. At the limit of large displacement the defect structure represents a nitrogen vacancy. The defect level is of π character and its separation from the conduction edge is calculated to be 1.39 and 1.38 eV for the 17- and 31-atom clusters, respectively, for the EXH calculation and 1.12 to 1.16 eV for the IEXH calculation. Detailed comparison of this vacancy problem with the similar defect in graphite is described eleswhere.[33]

It is interesting to compare the energy and charge distribution of such a defect as revealed by the truncated-crystal vs the SPC methods. Table II summarizes the results for the energy of the defect level and boron charges, as revealed by these methods. It is evident by inspection to Table II that the truncated crystal approach does not yield the proper location of the defect level with respect to the conduction band, and only approximate results are obtained. Due to the differences in geometry of the truncated clusters employed, the atomic charges carried by the nearest three boron atoms in the defect crystal orbital are not identical, as they should be. The perturbative effect introduced by the vacant site is propagating some 1–2 neighboring shells and introduces changes in the charge distribution of these coordination shells. Truncated-crystal models of the size used here are probably too small to account properly for such effects since the perturbations introduced by the edge atoms are also extended within 1-2 shells.

Similarly, a defect molecule approach considering only the first coordination shell is perhaps insufficient to account for the coupling of this level with the bulk crystal (compare the 1-shell and 4-shell results in Table II).

When model lattice relaxations are introduced on the three nearest boron atoms, the defect level shifts to 1.51 and 1.20 eV for inward and outward relaxations of 10% of the equilibrium perfect lattice bond length, respectively.

It should be mentioned that both in a nitrogen vacancy and in displaced carbon-impurity structures, the distribution of charge in the defect level is symmetrical with respect to the nearest three boron atoms, and the unpaired spin density in such levels should reveal an EPR signal with the same splitting pattern (10 peaks for ^{11}B crystal). The energy sep-

TABLE II. Calculated results for a nitrogen vacancy in hexagonal boron nitride, obtained using the EXH method. $E_{t\text{-}cb}$ denotes the energy difference between the conduction edge and the defect level. Q_{B1}, Q_{B2}, and Q_{B3} denote the boron π charge in the defect level. 7- 17- 31- 49-atom clusters correspond to 1, 2, 3, 4 coordination shells around the defect site.

	Truncated crystal			SPC			
Property	Cluster I	Cluster II	Cluster III	7 atoms	17 atoms	31 atoms	49 atoms
$E_{t\text{-}cb}$ (eV)	0.763	0.933	1.102	0.814	1.390	1.380	1.381
Q_{B1} (e)	0.482	0.481	0.435	0.721	0.572	0.572	0.571
Q_{B2} (e)	0.482	0.481	0.527	0.721	0.572	0.572	0.571
Q_{B3} (e)	0.482	0.475	0.527	0.721	0.572	0.572	0.571

aration between the defect level and the conduction band is somewhat higher for the vacancy (1.38 and 1.16 eV in EXH and IEXH calculations, respectively) than for the displaced carbon impurity (1.30 and 1.0 eV in EXH and IEXH calculations, respectively). Also, higher charge is accumulated on the boron atoms in the vacancy case (0.57e and 0.48e in EXH and IEXH calculations, respectively) than in the displaced carbon impurity case (0.36e and 0.29e in EXH and IEXH calculations for $R_C = 1.0$ Å). Due to the uncertainties in the semiempirical LCAO methods used, the absolute values of these calculated properties should not be given too much importance. The general features of these model defects are however believed to be correctly reproduced.

IV. ELECTROSTATIC POTENTIALS

The electrostatic effects introduced by either a nitrogen vacancy or a carbon impurity into the otherwise unperturbed lattice can be evaluated by solving the Poisson equation for the charge density $\rho(r)$ obtained from the electronic wave function Ψ of a finite BN cluster.

$$\nabla^2 V_{\text{elec}}(\vec{r}) = 4\pi\rho(\vec{r}), \tag{7}$$

where $\rho(r)$ is obtained from the N-electron wave function Ψ

$$\rho(\vec{r}_1) = \int \Psi^*(\vec{r}_1\vec{r}_2\cdots\vec{r}_N)\Psi(\vec{r}_1\vec{r}_2\cdots\vec{r}_N)d\vec{\tau}_1\cdots d\vec{\tau}_N. \tag{8}$$

The total electrostatic potential $V(\vec{r})$ is given by the sum of the electronic contribution [Eq. (6)] and the contribution from all the nuclei

$$V(\vec{r}_i) = V_{\text{elec}}(\vec{r}_i) + \sum_a \frac{Z_a}{|\vec{R}-\vec{r}_i|}, \tag{9}$$

where the wave function Ψ is formed from all occupied MO's. It has been recently demonstrated[61] that the electronic wave functions obtained from the self-consistent-field molecular-orbital (SCF MO) semiempirical approximations intermediate neglect of differential overlap (INDO),[28] reproduces quite accurately the electrostatic potential calculated from *ab initio* wave functions for medium-size molecules. When the atomic basis set employed by these LCAO methods is expanded in a Gaussian basis,[62] the Poisson equation can be analytically integrated.[63] Previous numerical methods[61,64] involved substantial errors in the potential near the nucleus and exceedingly large computation times. With the analytic method, we expand the Slater orbitals used by the INDO method as an atomic basis set in a series of gaussians (the 6-G expansion).[62] With this representation of the atomic basis set, the charge distribution $\rho(\vec{r})$ takes the form of a sum of contributions from the individual gaussians even in the multicenter case.[65] Computations of the electrostatic potentials for the unperturbed clusters I-III (Fig. 2) shows that in the region of the central BN bond the potential is unchanged within 0.1% when increasing the cluster size from cluster II to cluster III and changes only by 0.15% when passing from cluster I to cluster II.

In the case of neutral vacancy and neutral carbon imputity, the electronic eigenvalue problem necessitates open-shell SCF calculation, and the electronic density $\rho(\vec{r})$ is computed from contributions of both α and β spins, while in the unperturbed cluster this reduces to a closed-shell problem.

The use of many-electron self-consistent wave functions that already incorporate quantum exchange effects, for all the electrons in the cluster (including the "trapped" electrons that are treated as all other electrons in the *neutral* defect structures), suggests that the resulting potential should present a meaningful picture of the affinities of the various defects.

The electronic eigenvalue problem was solved for cluster I (Fig. 2) by standard INDO method for the perfect, N-vacancy and C-impurity structures. Charge density was then computed from the resulting wave function and the latter expanded in the 6-G expansion and used to solve the Poisson equation. The resulting electrostatic potentials along the line marked in Fig. 2, are presented in Fig. 4.

It is seen that upon introducing a carbon atom substituting at the site of a nitrogen atom, the electrostatic potential along the newly formed B–C bond is less attractive towards a negative point charge than the corresponding potential in the unperturbed structure, due to the lower affinity of carbon (electronegativity 2.5 on Pauling's scale) to attract electrons than nitrogen (electronegativity 3.0). The electrostatic effect is introduced by the carbon impurity is especially marked at the vicinity of the newly formed B–C bonds, while at the center of the hexagonal rings surrounding the impurity ($R = \pm 4.1$ a.u.) the potential is already very close to its value in the unperturbed structure.

When a nitrogen vacancy is formed, the electrostatic potential around the vacant site becomes very shallow, increasing thereby the affinity of this center towards capture of negative charge. The asymmetry of the potential around the center of the boron-vacancy bond ($R = 0.0$) is increased. Again, the perturbative effect introduced by the vacancy is already small at the center of the closest hexagons. Both the nitrogen vacancy and the carbon impurity in hexagonal boron nitride create thus acceptor states.

When a similar calculation is performed with the periodic 32-atom cluster the perturbative effect of both defects is seen to extend to a larger radius, and only after 2.5–3.0 Å away from the defect site

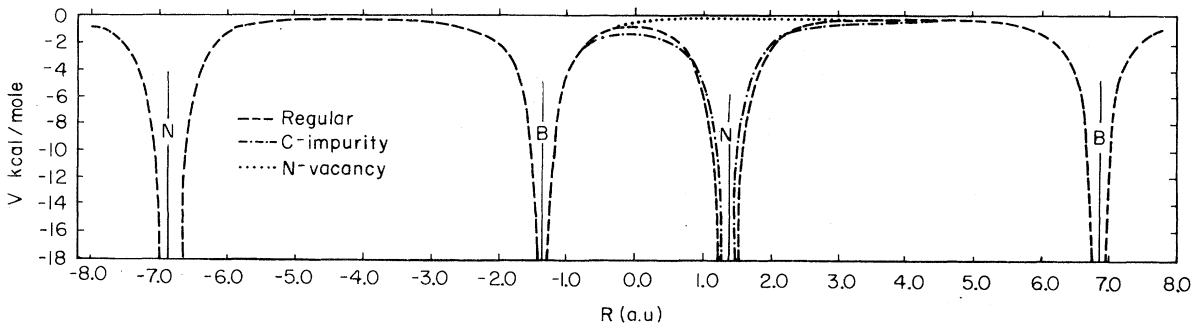

FIG. 4. Electrostatic potentials computed from INDO wave functions of cluster I along the vertical axis denoted in Fig. 2. R given in a.u. The potential describes electrostatic interactions with a positive point charge. The vacancy or the C impurity are placed instead of the nitrogen at 1.37 a.u.

the electrostatic potential approaches its value in the unperturbed lattice. Due to the presence of perturbations of edge atoms at this distance from the defect in the truncated-crystal models employed, the results obtained by these methods deviate significantly (Tables I and II) from those of the SPC model.

V. SUMMARY AND CONCLUSIONS

The electronic eigenvalue problem of a two-dimensional hexagonal D_{3h} lattice was represented by a minimal basis set of LCAO equations for a finite periodic array of hexagonally arranged atoms, exhibiting 2–4 orders of neighboring interactions. Semiempirical EXH and IEXH MO LCAO methods were used to facilitate the numerical solutions. For the ideal-lattice problem one thus obtains a subset of the eigenvalue spectrum of the infinite lattice that is sufficient to account for the various crystal band widths, band gaps, band-to-band transitions, equilibrium interatom distances, and atomic charge distributions. These calculated properties agree with the available experimental data.

The same method was then applied to the study of carbon impurity states. The main features obtained are (a) the appearance of a doubly degenerate σ level (4.9–3.2 eV below the conduction edge) and a singly degenerate π level in the forbidden gap, with a large degree of localization on the carbon site, and (b) formation on an extra defect π level that splits from the conduction band, when increasing the vertical distance of the impurity atom from the layer plane. This trapping defect level is associated with an even charge distribution on the three nearest boron atoms, and its separation from the conduction band is calculated to be 1.0–1.3 eV. Lattice relaxations around the carbon impurity defect were shown to stabilize the system by lowering the trapping level. Upon increasing the distance of the carbon atom from the layer to infinity, a nitrogen vacancy is formed. It was shown to be associated with a level that splits from the conduction band, and is situated 1.16–1.38 eV below it. An even charge distribution on the three nearest boron atoms is also manifested by this level. The effects of lattice relaxations were investigated as well as its coupling with the bulk crystal states.

In Paper I of this study a model was proposed to explain the results of EPR, luminescence, and glow-curve measurements on hexagonal boron nitride. The main features of the model were as follows: carbon impurities introduce an energy level at about 4.1 eV below the conduction band. Electrons may be excited from this level, pass through the conduction bands, and fall into traps. One such trap is a nitrogen vacancy. An electron trapped in the vacancy forms a three boron center (TBC), i.e., the charge is distributed equally on the three neighboring boron nuclei. This electron is trapped at about 1.0 eV below the conduction band, as revealed in glow curve measurements and in a "knee" at 600 °K in the isochronal annealing curves of the EPR signals (Paper I, Fig. 3). A second "knee" appeared at 800 °K, and it reveals the existence of another type of TBC, which was not observed in other measurements. In these centers electrons are trapped at about 1.4 eV below the conduction band (as can roughly be estimated from the "knee" in the isochronal annealing curve). This type of TBC may well be related to electron trapped in nitrogen vacancies, in the vicinity of carbon atoms.

The main features of the theoretical calculations are in good agreement with the model proposed to explain EPR, thermoluminescence, and thermally stimulated current measurements (see Paper I).

From the investigation of the characteristics of the calculation methods, it is concluded that: (a) truncated-crystal models with relatively small number of atoms should be treated with great caution when defect models are considered. The radius of the perturbative effects introduced by the defect should be estimated and kept well within the range where the edge effects of the truncated surface are

not important. (b) Defect-defect interactions present in the superlattice representation can be efficiently suppressed by using small periodic clusters of an odd number of primitive unit cells, keeping the interaction radius smaller than the molecular cluster radius, and seeking the convergence limit of the investigated electronic properties as a function of the interaction radius. This approach is useful in describing covalent defect structures exhibiting a reasonably short range electrostatic tail. A comparable interaction range is also sufficient to assure stability of the electronic and structural properties of the perfect lattice.

(c) The electronic affinity of various defect structures and its perturbation radius could be estimated by computing the Poisson potential generated by the quantum mechanically calculated charge density. This representation was previously successfully used in determining chemical reactivity of various molecules[61,63] and seems a promising technique for describing self-consistent potential rearrangement in defect problems.

(d) Due to the uncertainty underlying the semiempirical LCAO methods, one should examine the results yielded by several such methods since commitment to a single LCAO approximation might be misleading. The characteristics of both perfect lattice and defect structures are only semiquantitatively determined. However, the general features of these systems are clearly demonstrated. For more accurate results, *ab initio* methods are unavoidable.

[1]R. Taylor and C. A. Coulson, Proc. Phys. Soc. Lond. 65A, 834 (1952).
[2]A. Zunger, J. Phys. C 7, 76 (1974).
[3]A. Zunger, J. Phys. C 7, 96 (1974).
[4]C. A. Coulson and R. Taylor, Proc. Phys. Soc. Lond. A 65, 815 (1954).
[5]M. B. Khusidman and V. S. Neshpor, Poroshk. Metall. 10 (8), 72 (1970).
[6]G. D. Watkins, in *Radiation Effects in Semiconductors*, edited by F. L. Vook (Plenum, New York, 1968), p. 67.
[7]E. L. Elkin and G. D. Watkins, Phys. Rev. 174, 881 (1968).
[8]E. Doni and G. P. Parravicini, Nuovo Cimento A 63, 117 (1969).
[9]F. Bassani and G. P. Parravicini, Nuovo Cimento 50, 95 (1967).
[10]C. A. Coulson, M. A. Herraez, M. Leal, E. Santos, and S. Senent, Proc. R. Soc. Lond. A 274, 461 (1963).
[11]G. F. Koster and J. C. Slater, Phys. Rev. 95, 1167 (1954); 96, 1208 (1954).
[12]F. Bassani, G. Iadonisi, and B. Preziosi, Phys. Rev. 186, 735 (1969).
[13]K. H. Bennemann, Phys. Rev. A 137, 1497 (1965).
[14]B. S. Gourary and A. E. Fein, J. Appl. Phys. 33, 331 (1962).
[15]C. A. Coulson and M. J. Kearsley, Proc. R. Soc. Lond. 241A, 433 (1957).
[16]W. Kohn, in *Solid State Physics*, edited by F. Seitz and D. Turnbull (Academic, New York, 1957), Vol. 5, p. 258.
[17]W. Kohn and J. M. Luttinger, Phys. Rev. 97, 1721 (1955); 98, 915 (1955).
[18]J. D. Levine and S. G. Davison, Phys. Rev. 174, 911 (1968).
[19]M. B. Khusidman and V. S. Neshpor, Theor. Expt. Chem. 3 (2), 270 (1967).
[20]E. B. Moore and C. M. Carlson, Solid State Commun. 4, 47 (1965).
[21]R. P. Messmer and G. D. Watkins, Phys. Rev. Lett. 25, 656 (1970).
[22]R. P. Messmer and G. D. Watkins, Phys. Rev. B 7, 2568 (1973).
[23]C. Weigel, D. Peak, J. W. Corbett, G. D. Watkins, and R. P. Messmer, Phys. Rev. B 8, 2906 (1973).
[24]F. P. Larkins, J. Phys. 4, 3065, 3077 (1971).
[25]M. R. Hayns, Phys. Rev. B 5, 697 (1972).
[26]R. Hoffman, J. Chem. Phys. 39, 1392 (1963).
[27]R. Rein, N. Fukuda, H. Win, and G. A. Clark, J. Chem. Phys. 45, 4743 (1966).
[28]J. A. Pople and D. L. Beveridge, *Approximate M. O. Theories* (McGraw-Hill, New York, 1970).
[29]K. H. Johnson, J. Phys. C 3, 195 (1972).
[30]E. B. Moore and C. M. Carlson, Phys. Rev. B 4, 2063 (1971).
[31]G. D. Watkins and R. P. Messmer, in *Computational Methods for Large Molecules and Localized States in Solids*, edited by F. Herman, A. D. McLean and R. K. Nesbet (Plenum, New York, 1973), p. 133.
[32]R. P. Messmer and G. D. Watkins, in *Radiation Damage and Defects in Semiconductors*, Conf. Ser. No. 16 (Institute of Physics, London, 1973), p. 255.
[33]A. Zunger, J. Chem. Phys. (to be published).
[34]R. S. Mulliken, J. Chem. Phys. 23, 1833 (1955).
[35]R. Rein, H. Fukuda, H. Win, G. A. Clark, and F. E. Harris, in *Quantum Aspects of Heterocyclic Compounds in Chemistry and Biochemistry* (Israel Academy of Science, City 1969), p. 86.
[36]L. M. Roth and A. J. Bennett, *Proceedings of the Tenth International Conference on the Physics of Semiconductors, Cambridge, Mass.* edited by S. P. Keller, J. C. Hensel, and F. Stern, USAEC, Oak Ridge, 1970, p. 619.
[37]J. M. Andre, J. Chem. Phys. 50, 1536 (1969).
[38]D. L. Beveridge and I. Jano, J. Chem. Phys. 56, 4744 (1972).
[39]W. E. Rudge, Phys. Rev. 181, 1024, 1033 (1969).
[40]D. Brust, Solid State Commun. 9, 481 (1971).
[41]D. J. Stukel, R. N. Euwema, and T. C. Collins, Phys. Rev. 179, 740 (1969).
[42]G. Blyholder and C. A. Coulson, Theor. Chim. Acta 10, 316 (1968).
[43]T. L. Gilbert, in *Sigma M. O. Theory*, edited by O. Sinanoğlu and K. B. Wiberg (Yale U. P., New Haven, 1970), p. 244.
[44]R. Hoffman, J. Chem. Phys. 40, 2474 (1964).
[45]L. C. Cusachs and J. W. Reynolds, J. Chem. Phys. 43, S160 (1965).
[46]J. Zupan, Phys. Rev. B 6, 2477 (1972).
[47]R. Vilanov, C. R. Acad. Sci. B 272, 1066 (1971).
[48]K. Hamrin, G. Johansson, U. Gelius, C. Nordling, and K. Siegbahan, Phys. Sci. 1, 277 (1970).
[49]M. J. Cazaux, C. R. Acad. Sci. B 270, 700 (1970).
[50]S. Larach and R. E. Shrader, Phys. Rev. 104, 68

(1956).
[51]V. A. Formichev, Sov. Phys.—Solid State 13, 754 (1971).
[52]M. J. Rand and J. F. Roberts, J. Electrochem. Soc. 115, 423 (1968).
[53]Janaf International Thermochemical Tables, Los Alamos Report No. LA-2368, 1966 (unpublished).
[54]R. S. Pease, Acta Crystallogr. 5, 536 (1952).
[55]J. Goubeau, in *Boron Nitrogen Chemistry*, Advances in Chemical Series, No. 42 (American Chemical Society, New York, 1964), p. 87.
[56]A. H. Silver and P. J. Bray, J. Chem. Phys. 32, 288 (1960).
[57]A. Pullman, in *Sigma M.O. Theory*, edited by O. Sinanoğlu and K. B. Wiberg (Yale U. P., New Haven, 1970), p. 280.
[58]A. W. Moore and L. S. Singer, J. Phys. Chem. Solids 33, 343 (1972).
[59]S. Nagakura and J. Tanaku, J. Chem. Phys. 22, 236 (1954); 23, 141 (1954).
[60]J. A. Sussman, Proc. Phys. Soc. 79, 758 (1962).
[61]G. Giessner-Prettre and A. Pullman, Theor. Chim. Acta 25, 83 (1972).
[62]W. J. Hehre, R. F. Stewart, and J. A. Pople, J. Chem. Phys. 51, 2657 (1969).
[63]S. Subrenic, H. Weinstein, and R. Paunz, Chem. Phys. Lett. 20, 419 (1973).
[64]R. M. Stevens, J. Chem. Phys. 52, 1397 (1970).
[65]S. F. Boys, Proc. R. Soc. Lond. A 200, 542 (1950).